STRENGTH
AND PLASTICITY

Effect of Heat Treatment on Wire + Arc Additive Manufactured Aluminum 5356 Alloy: Mechanical Properties and Microstructure Correlation

N. Harshavardhana[a, *]**, S. P Sundar Singh Sivam**[a]**, Rahul Ryan Savio**[a]**, Ahin Honymon**[a]**,
V. Apramayan**[a]**, Gulshan Kumar**[b]**, and Ashish Kumar Saxena**[c]

[a] *Department of Mechanical Engineering, SRM Institute of Science and Technology, Kattankulathur,
Chengalpattu, Tamil Nadu, 603203 India*

[b] *Department of Mechanical Engineering, Birla Institute of Technology and Science, Dubai, UAE*

[c] *Centre for Innovative Manufacturing Research, School of Mechanical Engineering, Vellore Institute of Technology, Vellore,
Tamil Nadu, 632014 India*

*e-mail: harshavardhananatarajan@gmail.com

Received November 28, 2022; revised August 27, 2023; accepted October 16, 2023

Abstract—In this work, the aluminum 5356 (Al5356) component was fabricated by Wire Arc Additive Manufacturing (WAAM) process and subjected to heat treatment at three different temperatures i.e., 450, 525, and 600°C. Detailed mechanical and microstructural characterization was performed on the as-fabricated and heat-treated samples to correlate the change in mechanical properties with its corresponding microstructure. The mechanical properties were estimated using the tensile and Rockwell hardness tester, and the microstructural characterization was performed using Scanning Electron Microscopy (SEM) and Electron Back-scattered Diffraction (EBSD) technique. The samples heat-treated at 450°C show superior strength (i.e. UTS 260 MPa) as compared to as-fabricated, heat-treated at 525 and 600°C due to the beneficial evolution of fine second phase particles after heat treatment.

INTRODUCTION

Additive manufacturing (AM) is a rapidly developing technique in the field of manufacturing, which can produce intricate shapes, small to large-size components with a faster production rate etc. Additive manufacturing (AM) showcases greater benefits over conventional fabrication processes due to its rapid manufacturing part-level customized design possibility. It could provide a huge advantage for the manufacturing industries, such as in the aerospace/ automobile sector [1, 2]. The AM process can be done either by powder or wire feed process [3]. The wire feed process has a higher deposition rate at a lower cost, higher material usage, and cheaper than the powder feed process. The fabrication of Aluminum 5xxx series (Aluminium-magnesium) alloys using the WAAM process recently gathered attention due to its applications in the aeronautical, shipbuilding, and automobile sector [4]. The Aluminum 5356 comes under the 5xxx series of alloys combined with 94% aluminum and 5% magnesium and the rest of the metals such as silicon, chromium, maganese, etc. Aluminum 5356 is widely used in modern industries due to its high strength-to-weight ratio, high ductility, weldability, formability, and corrosion resistance [5]. Pure aluminum has excellent pitting, corrosion, and oxidation resistance. However, it is prone to cracking. Hot cracking is also known as solidification cracking, and it mainly happens during the solidification of metals, resulting in susceptibility to welding [4]. On the other hand, Aluminum 5xxx series alloys have low crack sensitivity, good welding properties, excellent strength, good pitting resistance, corrosion and oxidation resistance, and low cracking under pressure. Table 1 shows the comparison of mechanical Properties of Al5356 alloys fabricated through casting and WAAM process. The WAAM process shows superior strength and ductility compared to conventional casting process.

The Aluminum 5xxx series alloys are considered non-treatable alloys, as the alloys are unstable with time at elevated service temperatures due to the formation of β-precipitation of Al_3Mg_2 particles [5]. The formation of the β-phase can initially result in an increase in the tensile strength and hardness followed by a decrease in the mechanical properties at an elevated temperature [9]. Thus, the investigation of heat

Table 1. Mechanical properties of Al5356 alloys fabricated through casting and WAAM process

Properties	Casting[6]	WAAM[78]
Tensile strength, MPa	200	265
Yield strength, MPa	120	215
Elongation at break, %	20—30	60—90
Hardness (HRB)	30—50	60—90

Table 2. Alloy composition in as-received Al5356 wire sample (in percentage)

Al	Mg	Mn	Cr	Si	Fe	Ti	Others
94.7	4.85	0.15	0.05	0.04	0.09	0.07	0.057

treatment on the Aluminum 5xxx series alloys plays a crucial role in understanding the effects of heat treatment on the mechanical and microstructure of Aluminum 5xxx series alloys fabricated using WAAM. These alloys are typically strengthened by substitutional solid solution and not by the presence of the iron and manganese aluminides. Iron is generally not added intentionally to Al5356 alloy due to its potential to form brittle intermetallic compounds. Iron can form iron aluminides when the alloy is subjected to high-temperature processing or heat treatment. These intermetallics can have a detrimental effect on the alloy's mechanical properties, making it more brittle. The formation of manganese aluminides in Al5356 alloys is not a primary concern due to the low manganese content in these alloys. The intentional alloying elements, such as magnesium, primarily influence the alloy's properties. The trace amounts of manganese impurities in Al5356 alloy can lead to the formation of manganese aluminides, which are intermetallic compounds of manganese and aluminum of obtaining the desired alloy characteristics.

Li C. et al. [11] developed Aluminium alloy with higher welding speed and smaller heat input using the WAAM process, followed by post-heat treatment. The heat-treated samples show improved mechanical properties and enhanced microstructure due to the formation of second-phase particles with the uniform distribution of Si and Mg. In another study, Wang J. et al. found that the aluminum alloys fabricated through WAAM using cable-type welding wire (CWW) have better yield strength and average ultimate tensile strength than those made from the casting processes [10]. Li S. et al. [7] also showed the impact of shielding gas (i.e. nitrogen, (N_2), and argon (Ar)) on the shape and size of the weld bead and microstructure in Al5356 alloys. After fabrication, the Nitrides present in the sample would improve the microhardness but reduce the ultimate tensile strength. The N_2 shielded sample was subjected to a combined brittle and ductile fracture, while Ar shielded samples experi-

enced only ductile fracture [7]. The addition of impurities such as titanium with Al5356 alloy results in improved mechanical properties and a change in grain morphology from columnar to equiaxed structures [12]. The double-pulsed directed energy deposition reduces equiaxed grain size from 36 to 21 μm, increasing the mechanical properties of Al−Mg alloys [13]. The as-deposited 5356 aluminum alloy using WAAM mainly contains α-Al phase and β-Al_3Mg_2 phase in Al5356 alloys [14]. The formation of other phases, such as $Al_{0.56}Mg_{0.44}$, is due to the low solubility of magnesium in aluminum [15].

In summary, much work has already been done to optimize the WAAM parameters and environment conditions for Al5356 alloy [2, 7, 12, 13, 16]. However, to the author's best knowledge, the post-processing heat treatment of the Al5356 WAAM component has not been discussed in published literature concerning microstructural development and mechanical properties. The investigation of post-heat treatment on the mechanical and microstructure of Al5356 alloy plays a crucial role in understanding the structure-property correlation. So this current study focuses on the fabrication of Al5356 alloy using the WAAM process followed by heat treatment at 450, 525, and 600°C on fabricated components. Further, a correlation of mechanical properties and microstructure is made to select suitable heat treatment for Al5356 alloy.

EXPERIMENTAL

Material and Chemical Composition

The commercially pure Al5356 wire of diameter 1.2 mm was obtained from our industrial partner. The alloy composition of the wire alloy sample is shown in Table 2. The wire was certified and met industry standards for chemical composition, mechanical properties, and microstructure for Wire Arc Additive Manufacturing (WAAM). The ESAB Autrod 5356 Aluminium MIG welding wire spools are used in our study [17].

Component Fabrication Using WAAM

The wire arc additive manufacturing of the Al5356 alloys component was fabricated using Kemppi double pulse X8 MIG Welder, which is controlled using Wise Fusion software for optimal short-circuit characteristics in pulsed MIG welding [18]. The Kemppi double pulse X8 MIG Welder is assembled on the Yasaka 6-axis automatic robot. The completed set up includes Kemppi double pulse X8 MIG, wire feeding system, argon gas shielding system, etc., as shown in Fig. 1a. The M/s Kemppi uses "WeldEye" Welding management software to ensure consistent and effective argon gas flow rate and pressure for shielding throughout the welding process. The gas flow rate and pressure were set according to the 'WeldEye welding management software developed by M/s Kemppi Systems, and it is
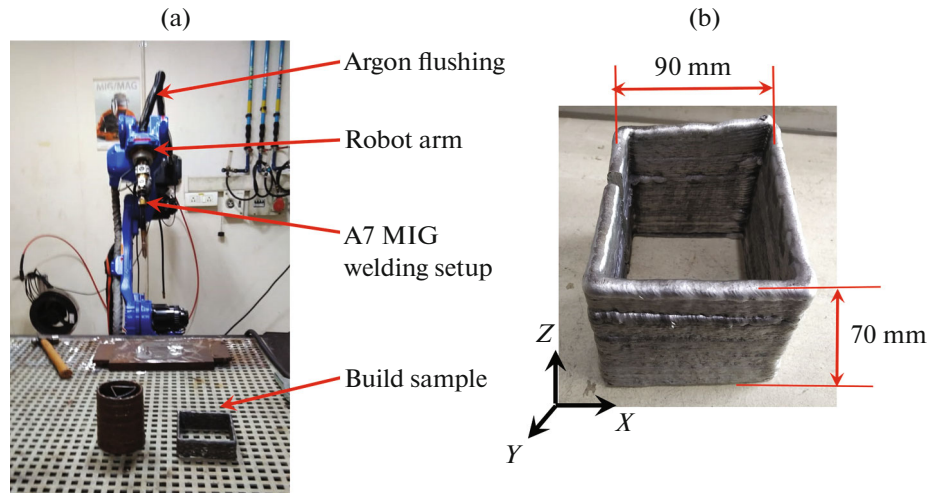
Fig. 1. (a) Wire arc Additive Manufacturing (WAAM) setup (b) fabricated Al5356 component using WAAM.

known for its high-quality welding performance and advanced features, such as automatic gas control and monitoring systems. The Al5356 wire of diameter 1.2 mm was used as the filler metal, and the pure aluminum plate with dimensions of 125 mm × 100 mm × 6 mm (length × width × thickness) was used as the base plate. To ensure uniformity in the layers, the combination of process parameters such as current, voltage, wire feed speed, and travel speed were set according to the "WeldEye" Welding management software. We carefully adjusted these parameters based on our previous experience and "WeldEye" Welding management software to achieve a stable and consistent welding process. The process parameters for fabricating Al5356 material are shown in Table 3.

Figure 1b shows the final Al5356 as-fabricated WAAM sample. The X, Y, and Z direction in the fabricated sample is shown in Fig. 1b. At first, the Al5356 wire was melted by the X8 MIG Welder and then solidified on the base metal to get the first layer. The process is repeated for 80 passes to obtain the Al5356 component. The final component consists of a square wall structure with dimensions 90 × 70 × 8 (width × length × thickness) deposited with no adjacent/ support layer, as shown in Fig. 1b. The travel direction of each layer is from left to right and was parallel to the previously deposited layer. We used inter-pass cooling to control the temperature and prevent overheating during welding, which can lead to distortion, cracking, and other defects. The inter-pass timing was set as 1 min to allow cooling between layers. The inferred cooling rate of aluminum in the natural air is about 11°C/s and the inter-pass time of 1 min is set to ensure the sample reaches near room temperature from molted temperature (approx 700°C) and the microstructure and mechanical properties of the material were not negatively affected by excessive heating or cooling. In addition, we monitored the temperature using a thermal image camera and controlled the cooling rate by adjusting the welding cooling time and temperature.

The deposition torch tip to workpiece distance was kept to 15 mm, and the contact angle was 90° for all the experiments.

Heat Treatment, Mechanical, and Microstructure Characterization

After fabrication, samples of were cut from the selected areas using wire-cut Electrical discharge machining (EDM) for hardness, tensile strength, and heat treatment. The specimens were cut using a wire-cut EDM in horizontal (along the X direction) and vertical (along the Z direction) directions under constant cooling with a water-based coolant, which avoids any potential effects of anisotropy. Additionally, both fabricated and heat-treated samples were cut from the same fabricated component to ensure consistency in the testing.

The heat treatments of the fabricated component were performed at three temperatures 450, 525, and 600°C in a muffle furnace. The specimens were placed in the furnace, and once the desired temperature was

Table 3. Process parameters for Wire arc Additive Manufacturing (WAAM) for fabricating Al5356 Alloys

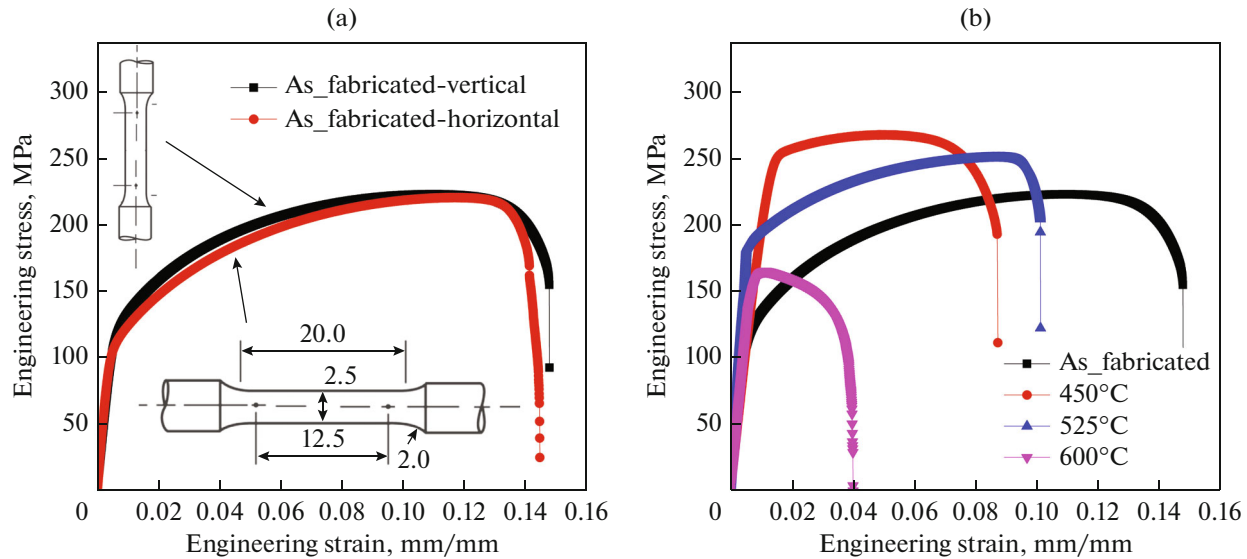| S. no	Process parameters	Values
1	Welding type	Double pulse
2	Wire feed rate	4.9 m/min
3	Welding speed	4.2 m/min
4	Average current	97 A
5	Voltage	19 V
6	Shielding gas	Argon

Fig. 2. Engineering stress-strain behavior (a) as-fabricated sample cut along in horizontal and vertical directions (b) as-fabricated sample and heat-treated samples at 450, 525, and 600 for 2 h.

reached, the specimen was held in the furnace for 120 min holding time. After heat treatment, samples were removed from the furnace and cooled in the ambient air.

The tensile testing on multiple specimens for each of the material's state ensures statistical significance and minimize the effect of any possible variability. Samples were tested with four specimens for each of the material's states, including as-welded, heat-treated conditions. To obtain the mechanical behavior of materials, tensile tests were carried out on dog-bone samples as per the ASTM E8 [19], and the standard dimensions dog bone sample is shown in Fig. 2. The tensile tests were performed at room temperature at a constant strain rate of $10^{-4}\,s^{-1}$ using an Instron 5K tensile testing machine with Epsilon Model 3542 Axial extensometer. The samples pulled between two mechanical grippers and the engineering stress-strain were plotted for mechanical properties such as yield strength, ductility, and ultimate tensile strength (UTS). The hardness measurements (as per ASTM E18 standard) were carried out on a mirror-polished surface on the Rockwell B (HRB) scale using a 1/16" ball indenter at the major load of 150 Kgf and kept under load for 15 seconds dwell time [20]. Hardness measurements were carried out along the length of the sample at various locations to obtain the average hardness value. We have taken two to three indentation per points for checking the repeatability of data. In addition, indents were at least 3 mm from the edge of the sample.

For the SEM micrograph, samples with mechanically mirror-polished surfaces were chemically etched for 10 s with an etchant solution made up of HF, HNO_3, and deionized water at 1 : 3 : 46, respectively.

The etchant sample was examined with a high-resolution Scanning Electron Microscope (HR-SEM) of JEOL, Japan, equipped with an Energy Dispersive Spectrometer (EDS). The X-Ray Diffraction (XRD) was performed on the polished samples using the Bruker USA D8 Advance Davinci X-Ray Diffractometer machine with an angle of 20° to 90°. Copper (Cu) K-alpha radiation is used in X-ray sources. The XRD peak data was analyzed using Xpert Software to identify various peaks. The EBSD was performed on *Y–Z* planes in FEI Quanta-200HV SEM, and data was analysed using the TSL-OIM™ software package. The samples were mechanically mirror-polished surface by using 220, 400, 600, 1000, 2500, and 4000 grade SiC papers using the conventional route followed by diamond polishing with 1 μm grade diamond paste with HIFIN@ as a lubricant at the rotation speed of 300 rpm. Finally, samples were polished with VibroMets 2 vibratory polishing machine and Mastermets 2 suspension for about 8 h. In EBSD, total area of 500 μm × 500 μm was covered with a step size of 0.6 μm to obtain sufficient statistics about grain orientations. All-grain boundaries were identified based on the 15° misorientation criterion—i.e. continuous presence of more than 15° boundary demarcates a grain. From such grains, the average grain size for a sample and the distribution of grain sizes were estimated.

RESULT AND DISCUSSION

Mechanical Properties of Al5356 Sample

Tensile tests were performed on 450, 525, and 600°C heat-treated samples at room temperature and compared with the as-fabricated WAAM sample.
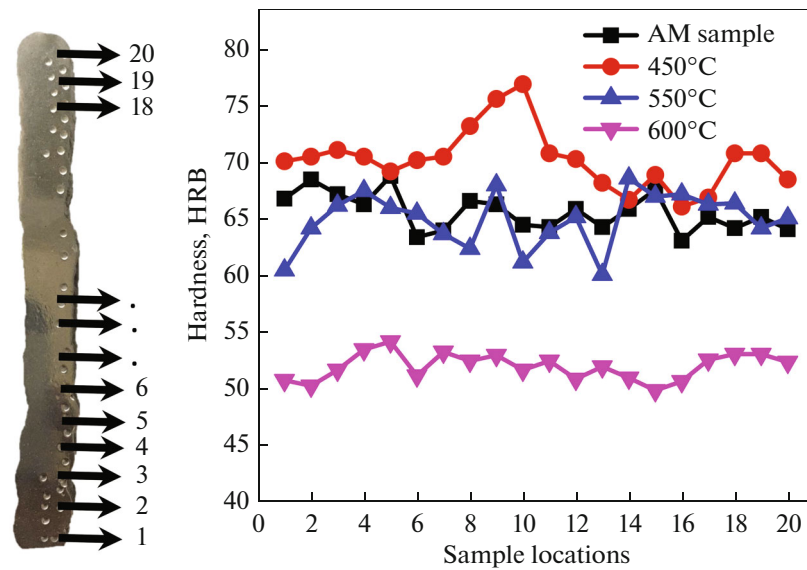
Fig. 3. Variation of the hardness at various locations for as-fabricated, 450, 525, and 600°C heat-treated samples for 2 h.

Figure 2a shows the engineering stress-strain behavior of as-fabricated WAAM samples cut horizontally (along the X direction) and vertically (along the Z direction). The yield strength value and the UTS for both vertical and horizontal samples show approximately the same value of around 120 and 210 MPa, respectively. Hence, we only report results from the vertical (along the Z direction) samples. Figure 2b shows the engineering stress-strain behavior of the as-fabricated sample and all heat-treated samples. Figure 2b shows that the as-fabricated sample has high ductility and low strength, while 450°C heat-treated samples show the highest tensile strength of 252.5 MPa compared to the as-fabricated one. In other heat treatments at 525°C, the tensile strength value reduces to 175 MPa with slightly more ductility than 450°C heat-treated samples. After heat treatment at 600°C, both tensile strength and ductility significantly decreased compared to all other cases.

Figure 3 shows the hardness variation at different locations from bottom to top for the as-fabricated samples and samples heated at three different heat-treated conditions. The as-fabricated Al5356 sample shown on the left of Fig. 3 indicates various locations of hardness measurements, where the location number starts from the bottom to the top (1−20). Table 4 shows the average hardness and standard deviation for as-fabricated, 450, 525, and 600°C heat-treated samples for 2 h. The as-fabricated WAAM samples show an average hardness value of 65.61 HRB at various locations of the sample. For the 450°C heat-treated samples, there is a significant increase in hardness at multiple locations. The peak hardness reaches 75 HRB with an average hardness of 70.29 HRB. As the heat treatment temperature increases to 525°C, there is a slight decrease in hardness to 64.95 com-

pared to the 450°C heat-treated samples. Finally, the 600°C heat treatment sample shows a significant drop in hardness to about 52HRB compared to other heat-treated samples.

Microstructure Analysis

The SEM micrograph of the as-fabricated sample along the $Y−Z$ direction at the bottom, middle, and top regions is shown in Fig. 4. From the SEM micrograph, it is clear that there is no considerable difference in microstructure at the bottom, middle and top regions. The yellow arrow indicates that the second-phase particles appear all over the surface at various locations. The grain boundaries are not revealed in the SEM micrograph. So EBSD was carried out on the as-fabricated and heat-treated samples to understand the correlation of mechanical properties concerning grain morphology, orientation, and the second-phase particles.

Figures 5a−5c show the SEM image, inverse pole figure (IPF) map, and Image quality Maps (IQ), respectively, from EBSD of the as-fabricated Al5356 alloys (in $Y−Z$ direction). Figure 5a shows that the

Table 4. Average hardness standard deviation for as-fabricated, 450, 525, and 600°C heat-treated samples for 2 h

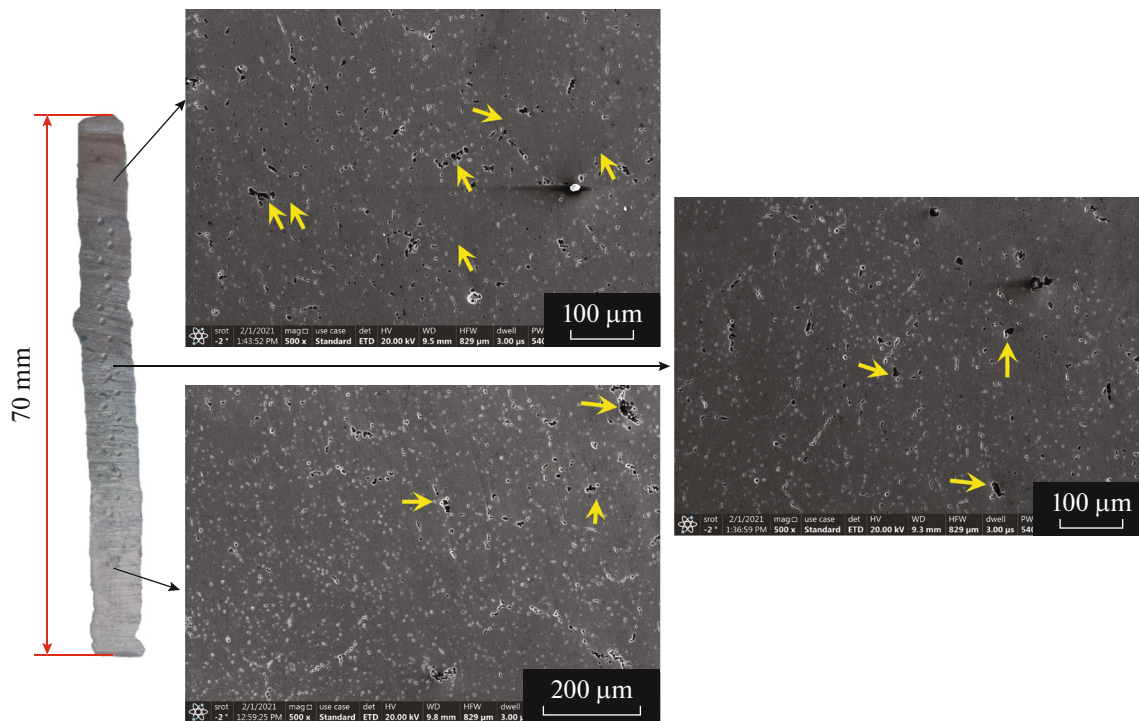| Conditions	Average hardness (HRB)	Standard deviation
As-fabricated	65.61	1.648
450°C	70.29	2.662
550°C	64.95	2.442
600°C	52.02	1.185

Fig. 4. The SEM micrograph of the as-fabricated sample along the $Y-Z$ direction at the bottom, middle, and top regions. The yellow arrow indicates the presence of precipitates.

SEM image which differentiates between the aluminum phase and second phase particles. The EDS spot analysis shows the presence of Al−Mg elements which is β secondary particles, whereas the base material only shows Al and Mg elements. The EDS spot analysis at three different location shows Mg rich precipitate at (1) and (2), comparted to primary α-Al phase. The EDS spot analysis at (3) shows the presence of primary α-Al rich phase as shown in table in Fig. 5. The microstructure shows the β second phase particles, which contribute 9.9% of the area fraction (marked with an arrow), and the grain boundaries are not visible in the backscattered SEM micrograph. Figures 5b and 5c show inverse pole figure (IPF) and image quality (IQ) maps, respectively, for as-fabricated samples in the $Y-Z$ plane. All boundaries with more than 15° misorientation were marked with black lines and were considered grain boundaries. The grains appear to be elongated along the Z direction with second-phase particles (black color spot), as shown in Fig. 5c. The marked boundaries include both grain and twin boundaries. The colors in the IPF map indicate the orientations of the individual grains according to the accompanying color map (see insert). In Fig. 5b, the presence of all oriented (111), (110), and (100) grains indicates the random texture in the as-fabricated sample. The average grain size of as-fabricated Al5356 alloys was found to be big (~83.3 ± 27.4 μm) with the presence of second-phase particles. The same

procedure is repeated for microstructure analysis of samples heat-treated at 450, 525, and 600°C.

Figure 6 shows the SEM image and Energy dispersive spectrometry (EDS) maps for the 450°C heat-treated sample. The SEM image revealed the presence of two main phases: a light one, a primary α-Al phase, and the secondary phases, which are intermetallic compounds (Fig. 6). The second phase is an Mg-rich intermetallic phase since other elements, such as Fe, Mn, etc., are in small amounts. The EDS spot analysis at two different secondary phases precipitates (1) and (2) and primary α-Al phase (3)shows the presence of rich in Mg atom compared to the primary α-Al phase, which results in Al−Mg β-secondary particles and primary α-Al phase comprised of Al and Mg elements respectively. The Table in Figure 6 shows the composition of secondary phase precipitates and primary α-Al phase. The Mg atom in β-secondary particles is relatively higher in β-secondary particles compared to the primary α-Al phase. The second phase particles mainly contain Al and Mg, which constitute the Al3Mg2 phase. Due to their shallow content, the EDS did not detect Fe, Si, and Mg in Al5356 alloys. A possible explanation is that the Fe, Si, and Mg, present in a very low range, dissolved in the grain boundaries.

Figure 7, the backscattering image differentiates the aluminum matrix from other second-phase particles. The 600°C heat-treated sample shows the grain boundaries (refer to the red arrow in Fig. 7); however, as-fabricated, 450, and 525°C heat-treated samples
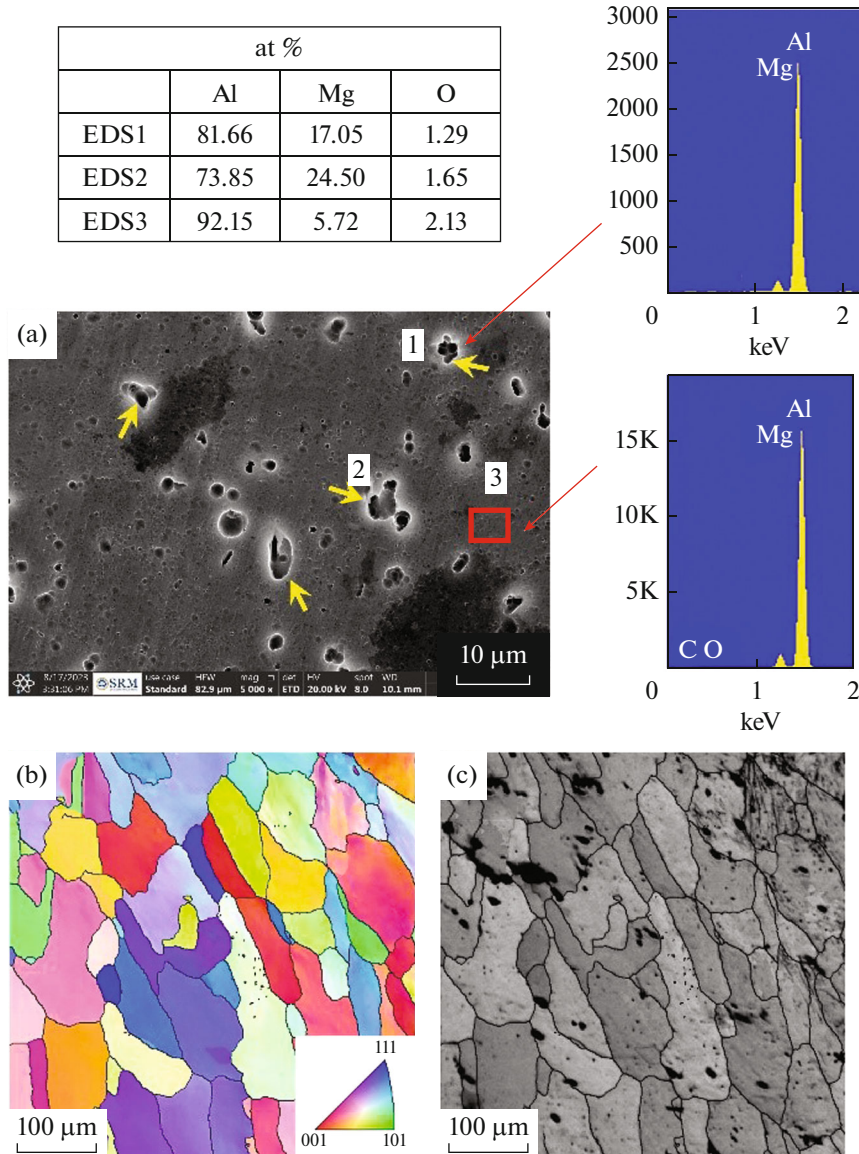
at %			
	Al	Mg	O
EDS1	81.66	17.05	1.29
EDS2	73.85	24.50	1.65
EDS3	92.15	5.72	2.13

Fig. 5. The (a) SEM image with EDS spot analysis, (b) inverse pole figure (IPF) map, and (c) Image quality Maps (IQ) from EBSD of the as-fabricated Al5356.

show the presence of second phase particles without grain boundaries after etching. Column (b) and (c) of Fig. 7 shows inverse pole figure (IPF) and Image quality (IQ) maps, respectively, for 450, 525, and 600°C heat-treated samples. The grain size of the 600°C heat-treated samples is higher than 450 and 525°C heat-treated samples. From Fig. 7, the size of the precipitate increases from 450 to 525°C, and it decreases at 600°C. The 450°C, has a smaller size and precipitate fine β phase particles resulting in higher hardness and tensile test of the sample. The 525°C heat-treated sample shows larger second-phase particles, which reduce the hardness and tensile strength of the sample. At 600°C, all the precipitate dissociates at grain boundaries, which results in low mechanical strength.

Figure 8 shows the variation of area fraction of β second phase particles and grain size for the as-fabricated, 450, 525, and 600°C heat-treated samples. The grain size is calculated from EBSD data, and the area of the β-particles is calculated using SEM image and the Metalplus software. The area fraction of the as-fabricated sample is 9.9%. As the heat treatment temperature increases, the area fraction of second phase particles increases to 10.47% for 525°C heat-treated samples. However, at 600°C, the precipitate fraction reduces to 6.5% due to the second phase particles dissociating at the grain The average grain size of as-fabricated Al5356 alloys was 83.3 ± 27.4 μm. The grain size increases consistently till 525°C heat treatment temperature, which is about 98.43 ± 39.57 μm, but for the 600°C heat-treated sample, grain size
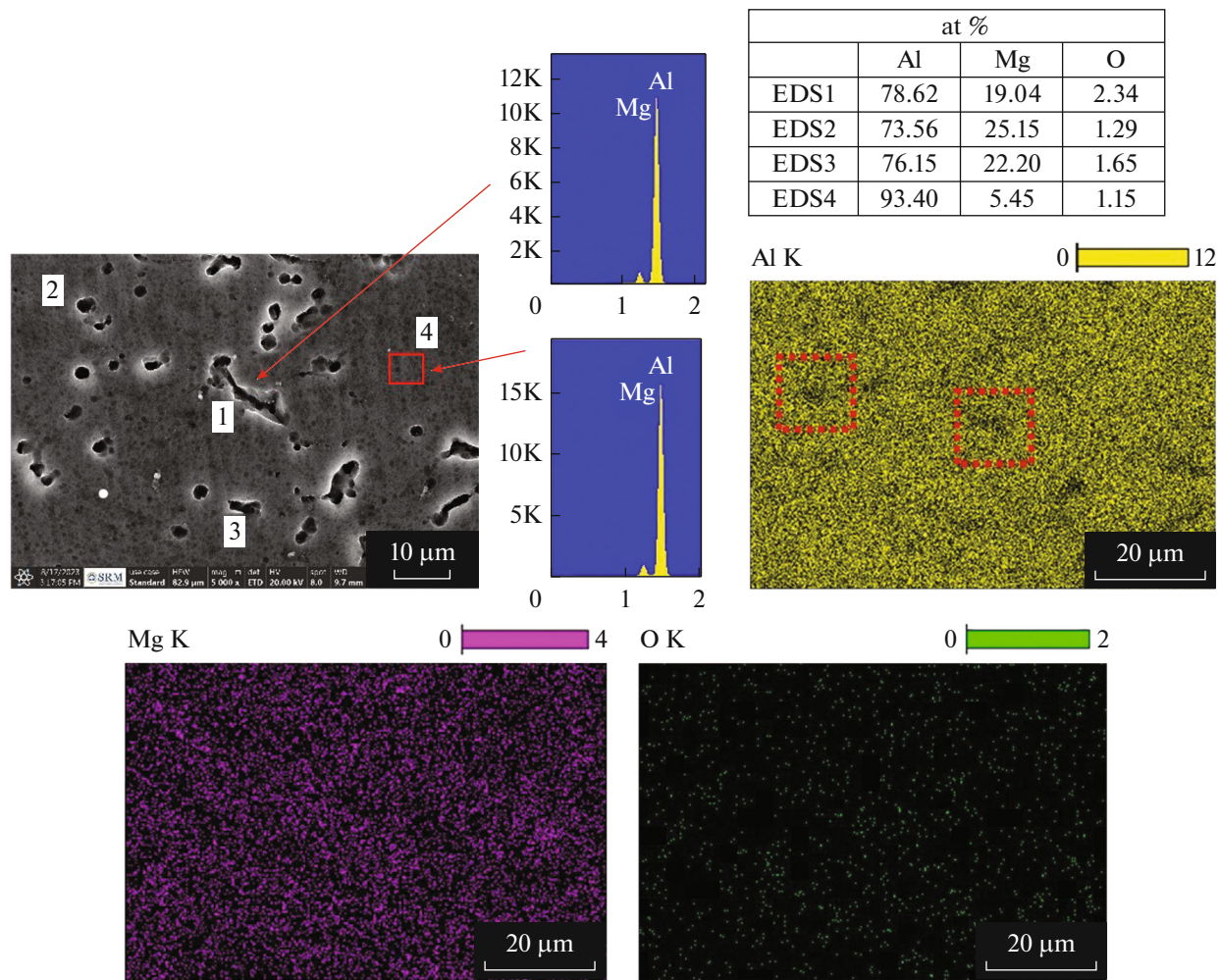
at %			
	Al	Mg	O
EDS1	78.62	19.04	2.34
EDS2	73.56	25.15	1.29
EDS3	76.15	22.20	1.65
EDS4	93.40	5.45	1.15

Fig. 6. The SEM micrograph of the 450°C heat treated sample sample along the $Y-Z$ direction.

abruptly changes to approximately 315 ± 125 µm. The grain size of Al5356 as-fabricated and alloys heat treated for 2 h is found to be in the range of 83.3 to 315 µm.

The corresponding 2θ value of the FCC Al matrix is 38.4, 44.7, 65.1, 78.23, and 82.4 which corresponds to (111), (200), (220), (311), and (222) *hkl* planes respectively. This Fig. 9 showed that the obtained spectral lines correspond to the fcc Al matrix shown in the circle at (1 1 1) and (200) and β-phase (Al_3Mg_2) at crystallographic planes at definite positions. The diffraction peak shows that the positions of Al and Al_3Mg_2 are almost the same, indicating that Al_3Mg_2 does not segregate significantly [10]. Due to the low volume fraction of the β-phase, the spectral lines were found to be weak peaks [21].

The lattice distortion results in increases energy and hinders the movement of dislocation within the crystal structure. This results in more resistance to plastic deformation and, in turn, enhances the material's yield strength, tensile strength, and hardness. The calculated lattice parameter of the Al-matrix alloy with varying magnesium concentrations is listed in Table 5, as shown below [4, 22]. The lattice parameter increases with higher concentrations of magnesium. This increase signifies lattice expansion due to the incorporation of magnesium atoms larger than aluminum atoms. The lattice expansion generates internal stress fields, creating barriers for dislocation motion and contributing to the solid solution hardening effect.

The heat treatment temperature was carefully chosen from typical Al−Mg Phase Diagram [23, 24], and heat treatment is performed at three different temperatures, say (1) 450, (2) 525, and (3) 600°C. When

Table 5. Variation of lattice parameter with magnesium concentrations in Al−Mg Alloys

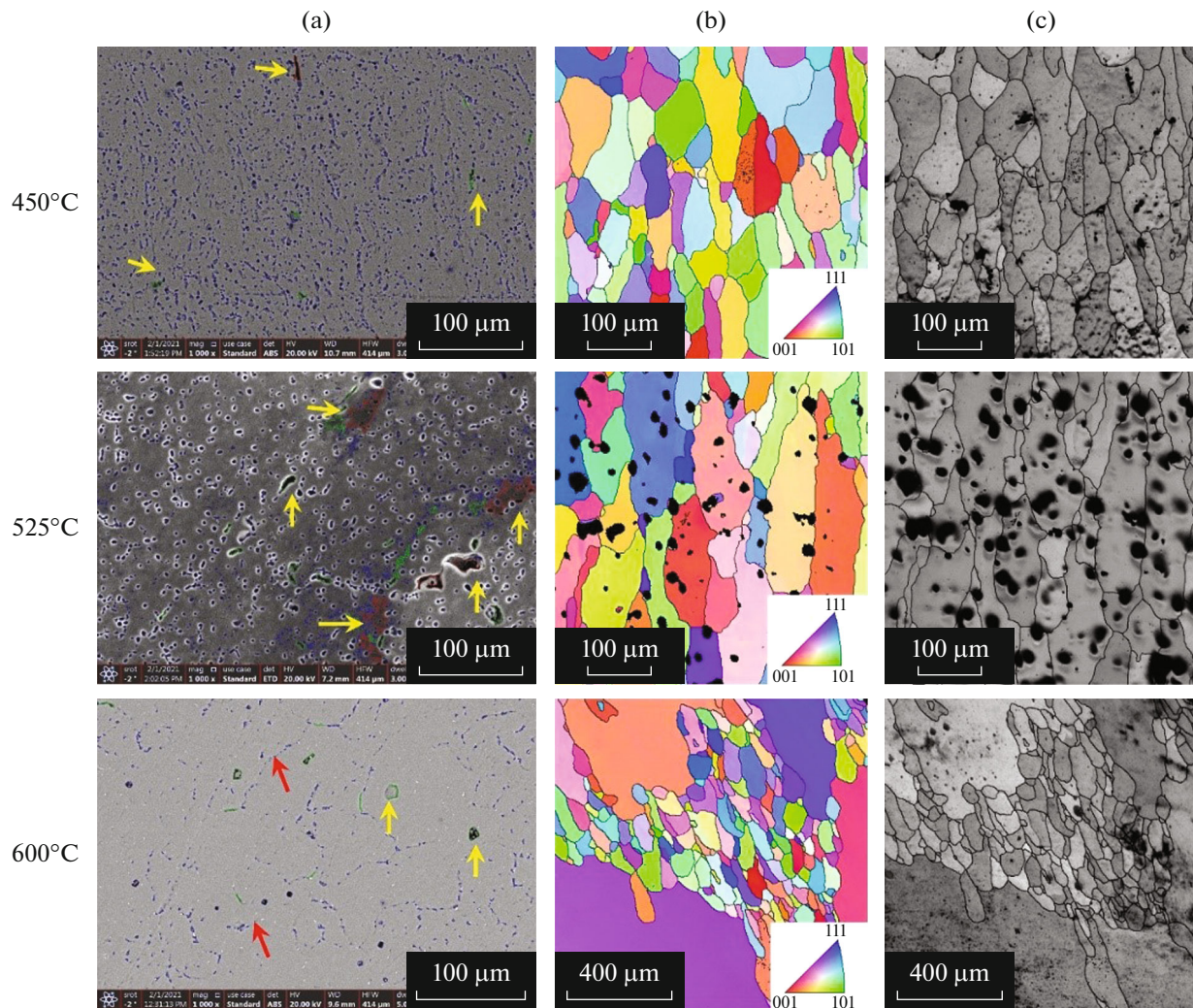| Mg concentration, %	Lattice parameter, Å
0 (Pure Al)	4.049
1	4.052
5	4.080
9	4.102

(a) (b) (c)

Fig. 7. The column (a) Backscatter SEM image, column (b) inverse pole figure (IPF), and column (c) Image quality (IQ) maps of the 450, 525, and 600°C heat-treated samples. The insert color indicates the different crystallographic orientation plane.
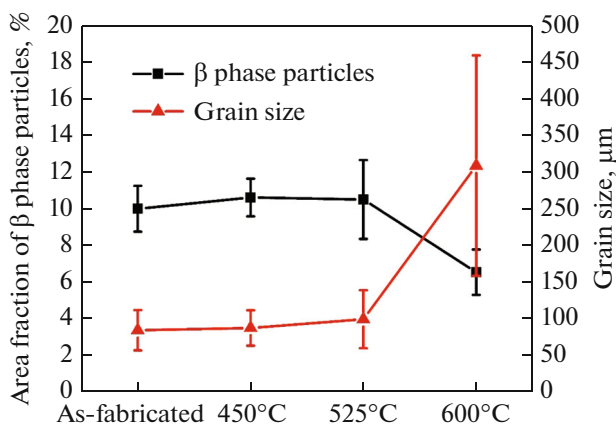

Fig. 8. Variation of area fraction of β second phase particles and grain size for the as-fabricated, 450, 525, and 600°C heat-treated samples from EBSD.
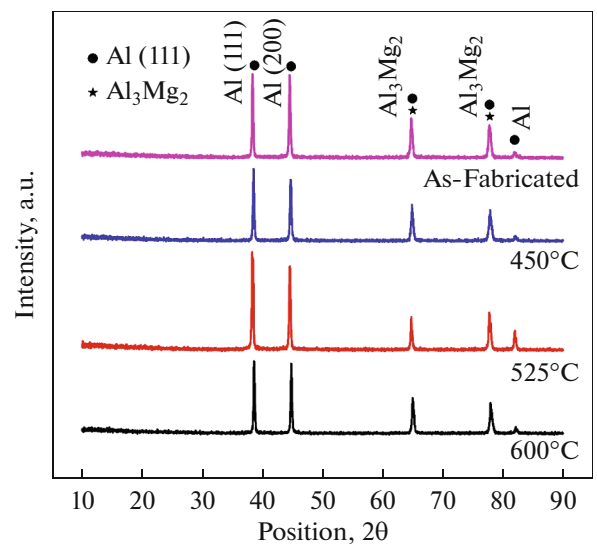

Fig. 9. X-ray diffraction (XRD) peak profile for as-fabricated, 450, 525, and 600°C heat-treated samples.

heated to 600°C, the samples result in the homogeneous single α phase, with most of the β phase formed during the WAAM process getting dissolved in grain boundaries (refer to Fig. 7). The sample heat-treated at 600°C shows less tensile strength and hardness at various locations, and the grain size of the sample increases compared to as-fabricated. On the other hand, the sample heat-treated at 450°C results in a fine β phase. Compared to other samples, the maximum hardening and tensile strength for a 450°C heat-treated sample is due to a fine dispersed β phase after heat treatment. The sample heat-treated at 525°C results in the coursing of the β phase, which decreases hardness and tensile strength compared to 450°C heat-treated samples. Although the β Al_3Mg_2 phase can be observed in the SEM and EBSD microscopy, the peaks are invisible in XRD for both as-fabricated and heat-treated samples. This is due to the low Area fraction of the β phase (less than 11%), and the β XRD peak is not detected [25]. The weak peaks also indicate the existence of other phases $Al_{0.56}Mg_{0.44}$, which resulted from the low solubility of Mg in aluminum [15]. Scudino et al. [21] showed that the low volume of β phase particles (i.e., less than 20%) results in the visibility of few and weaker peaks. As the β phase volume increases (i.e., 80%), diffraction peaks can be observed [21]. Zuo et al. [25] also show that aluminum alloys produced using the GTAW-based AM process shows many equiaxed grains with the second phase particles for the nonheated sample, and the grain size becomes coarser during different thermal cycles. The heat treatment improves average ultimate tensile strength and microhardness due to optimum second phase particles [25]. Also, as temperature increases (i.e., 600°C), β-Al_3Mg_2 phase dissolves into an α-Al phase which can result in revealing grain boundaries [25]. Su et al. showed that Al−Mg alloys manufactured using WAAM are stable with a stable microhardness throughout the height of the sample, followed by ductile fracture [26].

In summary, Al5356 samples fabricated using wire arc additive manufacturing gives stable microstructure and mechanical properties in both vertical and horizontal direction. The mechanical properties of the fabricated Al5356 samples can be improved by post-heat-treatment. The Al5356 samples, after heat treatment at 450°C for two hours, give superior tensile strength and hardness compared to the as-fabricated sample. As the heat treatment temperature increases (say 525 and 600°C), mechanical properties are reduced compared to 450°C heat-treated samples.

CONCLUSIONS

This study studied and correlated the fabrication of Al5356 aluminum alloys and the influence of heat treatment on the mechanical properties and microstructure. The following are the conclusions drawn from this study.

• Wire + Arc Additive Manufacturing (WAAM) is a complex manufacturing process that can produce components at a faster rate and manufacture near-net-shape components. The development of near net shape Al5356 alloy is possible using WAAM with the help of a double pulsed A7 MIG welding setup and optimizing the parameters such as voltage and current. The grain size of the as-fabricated samples was found to be 83.3 ± 27.4 μm.

• The post-heat treatment of the Al5356 component at 450°C gives superior mechanical properties compared to as fabricated, 525, and 600°C heat-treated samples. The formation of fine second-phase particles results in the superior properties of Al5356 alloys. As heat treatment increases to 525°C, the sample results in the formation, of course, second-phase particles, and at 600°C, second-phase particles move to the grain boundaries of the sample.

CONFLICT OF INTEREST

The authors of this work declare that they have no conflicts of interest.

REFERENCES

1. T. A. Rodrigues, V. Duarte, R. M. Miranda, T. G. Santos, and J. P. Oliveira, "Current status and perspectives on wire and arc additive manufacturing (WAAM)," Materials **12**, 1121 (2019).
https://doi.org/10.3390/ma12071121

2. M. Köhler, S. Fiebig, J. Hensel, and K. Dilger, "Wire and arc additive manufacturing of aluminum components," Metals **9**, 608 (2019).
https://doi.org/10.3390/met9050608

3. W. E. Frazier, "Metal additive manufacturing: A review," J. Mater. Eng. Perform. **23**, 1917−1928 (2014).
https://doi.org/10.1007/s11665-014-0958-z

4. K. S. Derekar, "A review of wire arc additive manufacturing and advances in wire arc additive manufacturing of aluminium," Mater. Sci. Technol. **34**, 895−916 (2018).
https://doi.org/10.1080/02670836.2018.1455012

5. J. R. Davis, "Introduction to aluminum and aluminum alloys," in *Metals Handbook Desk Edition* (ASM Inter-

national, 2001), pp. 417–423.
https://doi.org/10.31399/asm.hb.mhde2.a0003121

6. J. G. Kaufman and E. L. Rooy, *Aluminum Alloy Castings* (ASM International, 2004).
https://doi.org/10.31399/asm.tb.aacppa.9781627083355

7. S. Li, L.-J. Zhang, J. Ning, X. Wang, G.-F. Zhang, J.-X. Zhang, S.-J. Na, and B. Fatemeh, "Comparative study on the microstructures and properties of wire+arc additively manufactured 5356 aluminium alloy with argon and nitrogen as the shielding gas," Addit. Manuf. **34**, 101206 (2020).
https://doi.org/10.1016/j.addma.2020.101206

8. G. Saad, S. A. Fayek, A. Fawzy, H. N. Soliman, and E. Nassr, "Work hardening characteristics of gamma-ray irradiated Al-5356 alloy," Mater. Sci. Eng., A **607**, 132–137 (2014).
https://doi.org/10.1016/j.msea.2014.03.137

9. S. Sanamar, H. Brokmeier, and N. Schell, "Phase evolution of Al−Mg metal matrix composites during low temperature annealing at 200°C and 250°C," Intermetallics **124**, 106862 (2020).
https://doi.org/10.1016/j.intermet.2020.106862

10. J. Wang, Q. Shen, X. Kong, and X. Chen, "Arc additively manufactured 5356 aluminum alloy with cable-type welding wire: Microstructure and Mechanical Properties," J. Mater. Eng. Perform. **30**, 7472–7478 (2021).
https://doi.org/10.1007/s11665-021-05905-y

11. C. Li, H. Gu, W. Wang, S. Wang, L. Ren, Z. Wang, Z. Ming, and Yu. Zhai, "Effect of heat input on formability, microstructure, and properties of Al−7Si−0.6Mg alloys deposited by CMT-WAAM process," Appl. Sci. **10**, 70 (2019).
https://doi.org/10.3390/app10010070

12. D. Su, J. Zhang, and B. Wang, "The microstructure and weldability in welded joints for AA 5356 aluminum alloy after adding modified trace amounts of Sc and Zr," J. Manuf. Processes **57**, 488–498 (2020).
https://doi.org/10.1016/j.jmapro.2020.07.017

13. C. Ma, Yu. Yan, Z. Yan, Yo. Liu, X. Wu, D. Li, L. Zhao, P. Liu, and H. Jin, "Investigation of bypass-coupled double-pulsed directed energy deposition of Al−Mg alloys," Addit. Manuf. **58**, 103058 (2022).
https://doi.org/10.1016/j.addma.2022.103058

14. G. Saad, S. A. Fayek, A. Fawzy, H. N. Soliman, and E. Nassr, "Serrated flow and work hardening characteristics of Al-5356 alloy," J. Alloys Compd. **502**, 139–146 (2010).
https://doi.org/10.1016/j.jallcom.2010.04.119

15. Ya. Geng, I. Panchenko, X. Chen, Yu. Ivanov, and S. Konovalov, "Wire arc additive manufacturing Al−5.0 Mg alloy: Microstructures and phase composition," Mater. Charact. **187**, 111875 (2022).
https://doi.org/10.1016/j.matchar.2022.111875

16. M. Köhler, J. Hensel, and K. Dilger, "Effects of thermal cycling on wire and arc additive manufacturing of Al-5356 components," Metals **10**, 952 (2020).
https://doi.org/10.3390/met10070952

17. ESAB. Aluminium 5356 Wires Autrod.

18. M/s Kemppi. X8 MIG Welder (2022).

19. *ASTM E8/E8M standard test methods for tension testing of metallic materials. Annu. B. ASTM Stand. 4 ASTM E8* (2010).

20. *Standard Test Methods for Rockwell Hardness of Metallic Materials. ASTM Int. ASTM E18* (2015).

21. S. Scudino, G. Liu, M. Sakaliyska, K. B. Surreddi, and J. Eckert, "Powder metallurgy of Al-based metal matrix composites reinforced with β-Al$_3$Mg$_2$ intermetallic particles: Analysis and modeling of mechanical properties," Acta Mater. **57**, 4529–4538 (2009).
https://doi.org/10.1016/j.actamat.2009.06.017

22. A. Ahmed, S. Akl, and A. S. Hassanien, Int. J. Adv. Res. **2** (11), 1–9 (2014). https://www.journalijar.com/uploads/838_IJAR-4360.pdf.

23. J. L. Murray, "The Al−Mg (aluminum−magnesium) system," J. Phase Equilib. **3**, 60–74 (1982).
https://doi.org/10.1007/bf02873413

24. S. Bannour, K. Abderrazak, S. Mattei, J. E. Masse, M. Autric, and H. Mhiri, "The influence of position in overlap joints of Mg and Al alloys on microstructure and hardness of laser welds," J. Laser Appl. **25**, 032001 (2013).
https://doi.org/10.2351/1.4792615

25. W. Zuo, L. Ma, Yu. Lu, S. Li, Z. Ji, and M. Ding, "Effects of Solution treatment temperatures on microstructure and mechanical properties of TIG−MIG hybrid arc additive manufactured 5356 aluminum alloy," Met. Mater. Int. **24**, 1346–1358 (2018).
https://doi.org/10.1007/s12540-018-0142-3

26. Ch. Su, X. Chen, C. Gao, and Ya. Wang, "Effect of heat input on microstructure and mechanical properties of Al−Mg alloys fabricated by WAAM," Appl. Surf. Sci. **486**, 431–440 (2019).
https://doi.org/10.1016/j.apsusc.2019.04.255